# GF-4 Satellite Fire Detection With an Improved Contextual Algorithm

Ning Zhang, Lin Sun, and Zhendong Sun

***Abstract*—The GF-4 satellite has a moderate spatial resolution and is capable of high temporal frequency observation. Thus, it can play an important role in the acquisition of information regarding fires. In this article, the characteristics of brightness temperature difference between fire point area and nonfire point area are comprehensively analyzed. Employing the advantages of high-frequency continuous observation of these data, an improved algorithm for joint spatial attribute detection using multitemporal data is proposed. This method is based on the traditional contextual method and incorporates the concept of time sequence, and uses the changes in time phase before and after the fire to reduce the false alarm caused by the high heterogeneity of pixels in a single spatial scene in the traditional method. In order to evaluate the accuracy of the algorithm, the perfect moderate resolution imaging spectrometer thermal anomaly product is used as the verification data to evaluate the feasibility of the algorithm. At the same time, it is necessary to compare the algorithm in this article with the fire algorithm currently applied to GF-4 with the four typical regions. The improved algorithm shows better drawing ability, and the consistency of fire description of biomass combustion for many days is improved. In the case of the Heilongjiang region on October 30, 2017, the accuracy rate is improved by 62%, compared with the contextual method.**

***Index Terms*—Brightness temperature, fire point identification, GF-4, spatial characteristics, time phase change.**

## I. Introduction

LANDSCAPE combustion fires, including "wild fire" and "active combustion," widely interfere with the balance of the biological ecological environment [1]–[4]. The harmful gases and smoke released during fire combustion seriously affect the environmental climate and air quality [5]–[7]. For the unique high dynamic and decentralized characteristics of fire, the quantitative analysis of satellite observation technology has become the main means of detection [8]–[10].

Fire monitoring is performed mainly based on changes in temperature and reflectivity caused by the fire. Specifically, the differences in temperature and reflectivity between an area on fire and an area not on fire are used to detect the occurrence of fires. Fire point recognition methods, such as image enhancement method, threshold method (single threshold method, multithreshold method and dynamic threshold method), NDVI index method [11]–[13]. Fuchs *et al.* [19] were the first to use the Threshold Method based on mid-infrared and far-infrared channels to monitor fires. In this method, the discrimination threshold is set based on the surface temperature rise and the abnormal brightness temperature of mid-infrared and far-infrared channels when a wildfire occurs. This enables effective fire monitoring. However, owing to the relatively single condition, this method is more suitable for small fire spots. In different seasons, a single threshold condition cannot account for the seasonal changes in land surface temperature, and in some relatively complex areas, the land surface temperature cannot be divided according to the same standard. This leads to frequent false detection. NDVI index can be used as the reference index of fire combustion, but it cannot rely on the index to determine the fire. The complexity of surface types seriously affects the judgment of the index. With the launch of EOS/moderate resolution imaging spectrometer (MODIS), a complete MODIS fire point identification algorithm system and fire products have been formed, and MODIS fire point identification methods such as absolute threshold method, context algorithm and multichannel synthesis method have been developed [13], [20], [21]. Considering the influence of simultaneous interpreting of different parameters and different observation conditions on fire point recognition, a series of modified algorithm based on MODIS fire point recognition method is proposed. At present, the most commonly used fire detection algorithms are the Threshold Method and the contextual method [14]–[18]. Giglio *et al.* [20] proposed the contextual method and combined it with the original threshold method to improve the accuracy of fire point detection. The background radiation is obtained from the background window composed of the surrounding points of the point to be measured. This method uses the characteristics where the brightness temperature value of the mid-infrared and thermal infrared bands of the fire point pixel are significantly higher than that of the surrounding pixels, and detects the fire pixel according to the temperature difference between the fire point pixel and adjacent pixels. On the basis of the contextual method, Giglio *et al.* [21] and Freeborn *et al.* [22] proposed an improved method to compensate for the partial condition of sacrificing the information of small fire detection in the contextual algorithm and used the method for fire monitoring based on MODIS data. Considering influencing factors, such as direct sunlight, cloud-related effects, and coastal boundaries, the fire point algorithm incorporates cloud removal,

Manuscript received May 20, 2021; revised August 28, 2021 and October 10, 2021; accepted November 29, 2021. Date of publication December 3, 2021; date of current version December 23, 2021. *(Corresponding author: Lin Sun.)*

Ning Zhang and Lin Sun are with the College of Geodesy and Geomatics, Shandong University of Science and Technology, Qingdao 266590, China (e-mail: zhang_n20@163.com; sunlin6@126.com).

Zhendong Sun is with the Key Laboratory of Quantitative Remote Sensing in Agriculture of Ministry of Agriculture, Beijing Research Center for Information Technology in Agriculture, Beijing 100097, China (e-mail: szd2569733091@163.com).

Digital Object Identifier 10.1109/JSTARS.2021.3132360

desert boundaries, coastal boundaries, and solar flares. In the algorithm description of wildfire combustion monitored by GF-4 in recent years [23], [24], the contextual method has been adopted as the fire point location method, and the algorithms of most satellite products are also based on the contextual method, including VIIRS fire products currently in use [25]. As an important method of current fire detection algorithm, the contextual method meets the basic needs of fire detection to a certain extent. However, in areas with complex surface types, the judgment of a single spatial scene cannot completely eliminate the false fire alarm of high-temperature heterogeneous points. In areas with high spatial heterogeneity, there are significant differences in the distribution and change of surface temperature between adjacent pixels, and it is difficult for the contextual method to set an appropriate threshold to distinguish fire points and nonfire points. Therefore, it is difficult to eliminate false alarms in these areas, resulting in low fire point monitoring accuracy in such areas, for example, urban steel mills, solar photovoltaic power stations and other conventional hot spots [20], [26]. With the development of geostationary satellite, time series detection has become a new means of fire detection. The principle of most geostationary satellite fire detection algorithms is basically the same as that of earth orbiting satellite sensors [27], [28], which mostly depends on the setting of threshold. In current fire products, absolute brightness temperature or reflectivity value is usually used as the main condition for identification. The timing algorithm also uses the absolute change of brightness temperature in subpixel as the judgment condition. Time series algorithm has many uncertainties in its analysis method based on mean and continuous statistical values, and the mean ignores the main influencing factors of seasonal changes.

Hence, to improve the accuracy of fire point recognition in high-heterogeneity areas, this article proposes a multi temporal contextual method (MT-contextual). Using the temperature time difference analysis of multitemporal data, the spatial high -temperature heterogeneous points show a long-term high-temperature phenomenon in the long-time series, which is distinctly different from the short-term variability of fire. Therefore, it can solve the problem of low accuracy of fire point identification by the contextual method due to the differential distribution of spatial temperature. The method is applied to the fire point detection of the geostationary satellite GF-4. The characteristics of GF-4 satellite high-frequency observation provide a good application scenario for the multitemporal data requirements of this method.

## II. Input Data Characteristics

The GF-4 satellite is China's first geosynchronous orbit high-resolution remote sensing satellite. By leveraging the long-term stay of this satellite over a fixed area, high-efficiency remote sensing data acquisition can be achieved. This is available from the China Resource Satellite Center.[1] In this article, the data sources were GF-4 visible near-infrared multispectral cameras (PMS) and medium wave infrared (IRS) array cameras. The resolution of visible light and multispectral is better than 50 m, and the resolution of the infrared spectrum is better than 400 m [29]. For fire detection, the algorithm mainly uses the mid-infrared channel of the IRS sensor. The spectral response of the channel (ranging from 3.5 to 4.1 $\mu$m, centered on 3.8 $\mu$m) spans the peak spectral radiation wavelength of blackbody emitted under large temperature changes. It is highly suitable for distinguishing pixels containing sub-resolution combustion components from pixels composed of cooler flameless background areas. The other two band channels cover visible light (0.63–0.69 $\mu$m) and near-infrared (0.76–0.90 $\mu$m) areas to support cloud, solar scintillation and water identification in fire detection algorithms. The spectral and spatial characteristics of the channels used in this article are given in Table I.

*Image preprocessing*: RPC orthophoto correction, radiometric calibration and apparent reflectance calculation. The orthogeometric correction of Gf-4 PMS image is completed by rational function model, and the parameters used for radiometric calibration are provided by China Resources Satellite Application Service Center, the DN value of satellite image is converted into radiance image according to (1), and then the radiance value is converted into apparent reflectivity according to (2)

$$\mathrm{L}_e\left(\lambda_e\right) = \mathrm{Gain} \cdot \mathrm{DN} + \mathrm{Offest}. \tag{1}$$

*Including*: $\mathrm{L}_e(\lambda_e)$ is the radiance after conversion, and DN is the satellite load Measured value, $\mathrm{Gain}$ is the calibration slope and $\mathrm{Offest}$ is the absolute calibration coefficient displacement

$$\rho = \frac{\pi \cdot \mathrm{L}_\lambda \cdot D^2}{\mathrm{ESUN}_\lambda \cdot \cos\theta}. \tag{2}$$

*Of Which*: $\rho$ Is the relative reflectance of the ground, and $D$ is the solar terrestrial astronomical unit distance, $\mathrm{L}_\lambda$ is the spectral radiation value of the sensor, that is, the radiant energy of the top layer of the atmosphere; $\mathrm{ESUN}_\lambda$ is the average solar spectral radiation at the top of the atmosphere, that is, the solar irradiance at the top of the atmosphere, $\theta$ is the zenith angle of the sun.

## III. Algorithm Description

Based on verification analysis, fire detection algorithms and products of medium-resolution imaging spectrometers have been constantly updated and improved [30]–[34]. Most algorithms focus on the prominent mid-infrared pixels in a single scene and do not consider the fire characteristics in time series; this is because in some cases, the particularity of spatial heterogeneity leads to the misjudgment and omission of fire in a single scene, and the establishment of time series can effectively solve the problem of heterogeneous points in a single scene.

Thus, establishing time series is an effective method for modeling the temperature cycle of a target area. However, it is often difficult to collect long-term and effective time series data. Therefore, in this article, in order to improve the single scene algorithm and reduce the difficulty of long-term available time series data acquisition, a series model combining time and space is constructed. From the flowchart of the detection algorithm shown in Fig. 1, the idea of the algorithm can be understood

[1] [Online]. Available: http://www.cresda.com/CN/

TABLE I
SPECTRAL CHARACTERISTICS OF GF-4

| Type | Spectrum segment number | Spectral range (μm) | Spatial resolution (m) |
|---|---|---|---|
| Visible near-infrared | 4 | 0.63–0.69 | 50 |
| | 5 | 0.76–0.90 | 50 |
| Medium wave infrared | 6 | 3.5–4.1 | 400 |

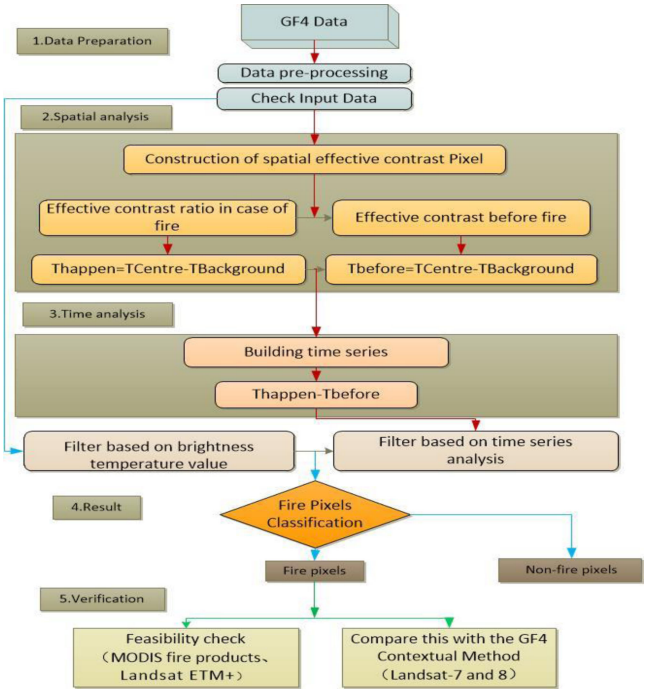


Fig. 1. Flowchart of fire detection algorithm based on GF-4 satellite data.

clearly. The output of the algorithm is a binary image, and the pixels are divided into "fire" and "no fire."

### A. Construction of Spatial Effective Contrast Pixels

In this article, the active fire detection algorithm of GF-4 is improved based on the contextual method, and attempts to use adjacent pixels to estimate the radiation measurement signal of potential fire pixels. Effective adjacent pixels in the window centered on potential fire pixels are identified and used to estimate the background value. By sampling the dynamically allocated window size, the best representation of the candidate fire pixel background was realized. In the case of GF-4 band, the minimum sample size was set to $12 \times 12$ element window centered on the candidate fire pixel. The sampling window is allowed to grow to a maximum size of $31 \times 31$ until at least 25% of the sample size is composed of valid pixels, or a minimum of eight valid pixels are found. Similar to large-area background sampling that is applied to data, effective pixels do not include pixels classified as clouds, potential background fire pixels (brightness temperature exceeds the initial threshold of 305 k) and pixels with nonzero quality flag on any input band, including pixels with filling value. If the minimum number of valid pixels cannot be met, the pixel was designated as an "unknown" class, indicating that the background condition could not be correctly characterized. In this article improves the algorithm, the distinctly abnormal data affected by cloud and water were deleted. The image is cloud processed according to the method that the pixels of optical thick cloud are independently classified and processed [Formula (3) (4)] formulated in the traditional International Geosphere Biosphere Program and MODIS fire products [20], [21]. Although the GF-4 satellite met the most basic algorithm input requirements, an important difference between the resolutions of the two sensors of GF-4 requires that resampling and orthophoto correction should be used for image registration before data use

$$\begin{cases} (\rho_r + \rho_n) > Th_{p1} \vee (T_{12} < Th_{t1}) \vee ((\rho_r + \rho_n) \\ \quad > Th_{p2} \wedge T_{12} < Th_{t2}) \ daytime \\ T_{12} < Th_{t1} \ night \end{cases} \tag{3}$$

$$(\rho_n < Th_{p3}) \wedge (\mathrm{NDVI} < 0)\,. \tag{4}$$

In (3) and (4), $\rho_r$ is the apparent reflectivity of the red band of the pixel; $\rho_n$ represents the apparent reflectance of a pixel in the near-infrared band; $T_{12}$ is the brightness temperature of the pixel in the thermal infrared band (because GF-4 has no thermal infrared band, the thermal infrared judgment condition can be ignored); $\mathrm{Th}_{p1}$ is the threshold value (the reference value is 0.9); $\mathrm{Th}_{p2}$ is the discrimination threshold (the reference value is 0.7); $\mathrm{Th}_{t1}$ is used as the threshold value (the reference value is 265k); $\mathrm{Th}_{t2}$ is the threshold value (285 k is the reference value); and $\mathrm{Th}_{p3}$ is the discrimination threshold (the reference value is 0.15). $\mathrm{NDVI}((\rho_n - \rho_r)/(\rho_n + \rho_r))$ is the normalized vegetation index.

### B. Calculation of Spatial Effective Contrast Pixels

After the spatial window pixels without invalid data are constructed, the pixel brightness temperature is compared between the window center pixel and the underlying surface pixel. In this article, the detection algorithm based on a single scene is as follows:

$$\begin{aligned} \Delta T_I &= T_i - T_{ib} \\ &= \frac{hc}{k\lambda} \frac{1}{\ln\left(\frac{2hc^2}{\lambda^5 L(\mathrm{fire})} + 1\right)} - \frac{hc}{k\lambda} \frac{1}{\ln\left(\frac{2hc^2}{\lambda^5 L(\mathrm{Adjoin})} + 1\right)} \end{aligned} \tag{5}$$

where $\Delta T_I$, $T_i$, and $T_{ib}$ are the temperature difference between the fire pixel and the background, the brightness temperature of the mid-infrared channel, and brightness temperature mean of adjacent effective pixels in mid infrared band, respectively; $C$ is the speed of light (m/s); $\lambda$ represents the central wavelength

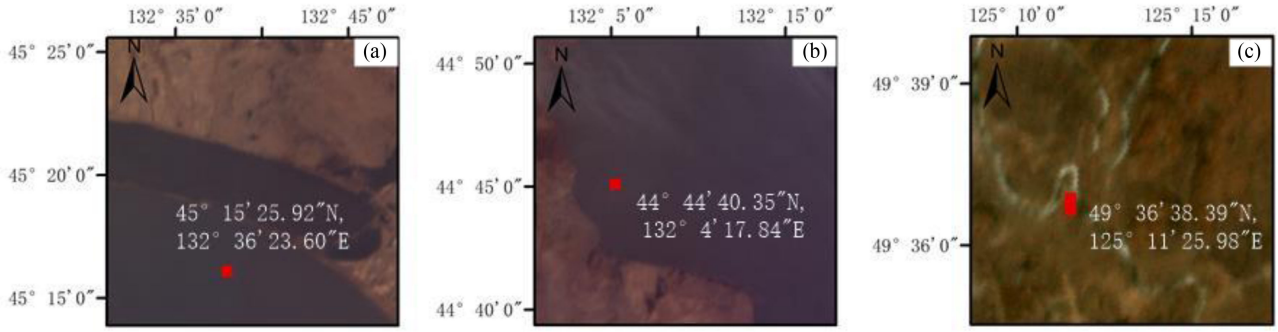


Fig. 2. Heterogeneous pixels in no-fire space. (a) October 24, 2017. (b) October 24, 2017. (c) April 9, 2017.

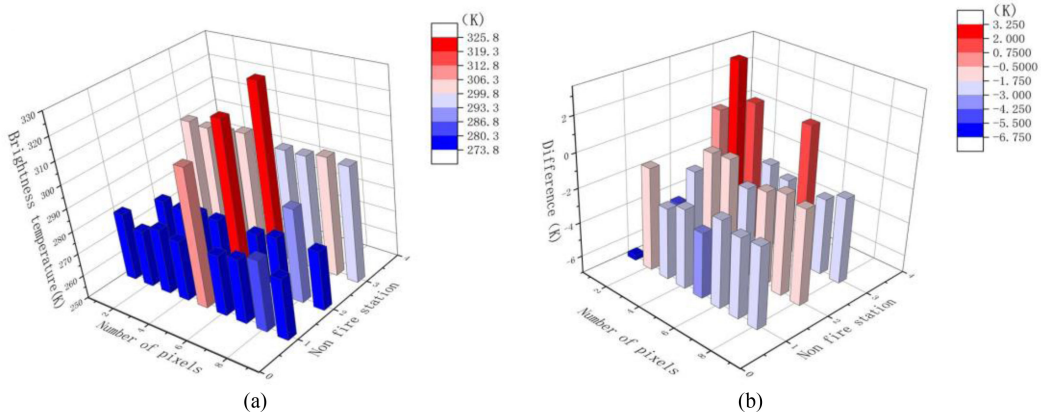


Fig. 3. Brightness temperature characteristics of nonfire spatial heterogeneous pixels.

($\mu$m); L is the radiance (W·m$^2$·sr$^{-1}$·um$^{-1}$); h is the Planck constant, with a value of 6.626 $\times 10^{-34}$j · s; and $k$ is the Boltzmann constant, with a value of $1.38 \times 10^{-23} J/K$.

### C. Calculation of Time Series

*1) Concept of Algorithm Design:* The contextual method provides an idea of fire identification, but the conditions of a single scene make it difficult to identify spatial heterogeneous points. To improve the limitations of the algorithm in a single scene, this article considers including a time series. The principle of most geostationary satellite fire detection algorithms is essentially the same as that of Earth orbit satellite sensors [35]–[38], most of which depend on the threshold setting. In current fire products, the absolute brightness temperature or reflectivity value is typically used as the main recognition condition [39]–[45]. The important theoretical component behind the algorithm investigated here is to compare the difference between the radiation value and the background radiation of the point to be measured at two different times, combining space and time for overall analysis, and considering that the comparison between the central pixel and the surrounding pixels is affected by outliers. In the algorithm, the brightness temperature of pixels difference obtained in a single scene continues to be compared in a time sequence.

For specific analysis three nonfire false alarm cases were selected for identification by the context algorithm. All false alarms were verified as nonfire high-temperature pixels through high-resolution images, and their spatial heterogeneity was analyzed. Their geospatial location is shown in Fig. 2. Fig. 3 analyzes the three false fire alarms. The pixel axis of Fig. 3(a) is the pixel number in the dynamic window of the corresponding station, and the station axis is the corresponding station of the three false fires in Fig. 2. At least eight effective comparison pixels are guaranteed in the dynamic window. The arrangement and numbering order of nine pixels including high-temperature heterogeneous pixels in the figure is from top to bottom and from left to right in the dynamic window. The vertical axis is the brightness temperature value of nine pixels in the dynamic allocation window. The figure demonstrates that the spatial high-temperature heterogeneous pixels show great differences from adjacent pixels, and the temperature of the central pixel was too high; indicating that the method of using only the abnormal bright temperature difference between the central pixel and the surrounding pixels as the basis for fire judgment is not stable; Fig. 3(b) depicts the change in the time sequence of the difference between the high-temperature pixel and the effective adjacent pixel in the window. The horizontal axis of the Fig. 3(b) represents the difference numbers of the corresponding central pixels and adjacent pixels of the three stations and stations, and eight effective difference numbers are obtained, still from top to bottom and from left to right. The difference between the central pixel and its neighboring pixel is computed initially, then the differences at varying times are subtracted and reported on the

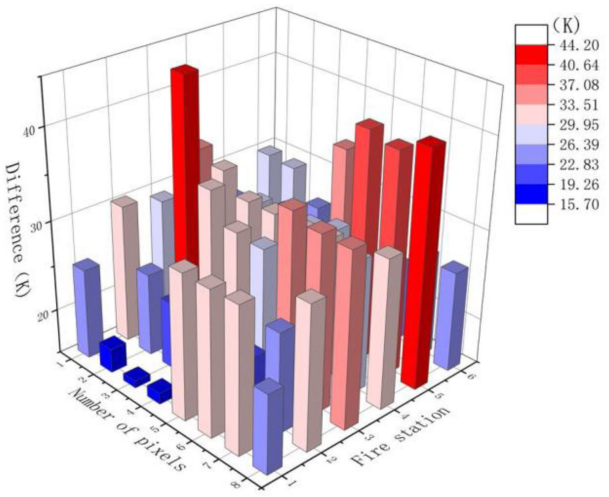


Fig. 4. Brightness temperature characteristics of fire pixels. The fire was selected on April 9, 2017 and verified by Landsat series satellite images, and the longitude and latitude information was 47° 58'31.58 "N, 124° 36'59.38" E; 47°49'25.48"N,125°13'47.57"E; 49°18'10.71"N,124°37'11.31"E; 49°17' 17.91"N,125°34'50.78"E; 49°17'17.91"N,125°34'50.78"E; 47°52'46.43"N, 124°32'45.06"E.

vertical axis. It can be seen from the figure that the difference between the central pixel and the surrounding pixels of nonfire spatial heterogeneous points does not differ greatly at different times, and the highest value is only 2 K. The analysis reveals that the causes of high-temperature heterogeneous points are rocks or bare land, dense human activities, factories and other areas in summer. Although these areas exhibit the characteristics of high brightness temperature, the brightness temperature value in the abnormal high-temperature area has no evident change in time sequence. Therefore, the judgment of time series improvement is less affected by special circumstances in the judgment of spatial heterogeneity.

In order to verify the stability of timing improvement, six fire cases were selected. Fig. 4 shows the characteristic analysis of pixels in the dynamic window of six stations. The horizontal axis is six station numbers, and eight effective difference numbers (the difference number between the corresponding central pixel and adjacent pixels of the station). They are arranged from top to bottom and from left to right in the dynamic window. The difference between the central pixel and its neighboring pixel is computed at first, then the differences at varying times are subtracted and reported on the vertical axis. The results show that the spatial difference between the two time periods is subtracted from each other, and the minimum value can still reach 15.7 k.

*2) Timing Establishment Cycle:* In the continuously updated time series algorithm, the time series algorithm often needs to build a long-term time series for comparative analysis. The establishment cycle of the time series needs to consider the impact of seasonal changes on the surface temperature (the surface temperature will rise relatively in summer). Therefore, the usual time series algorithm will describe the construction cycle suitable for subsequent use to avoid the impact of fire identification. It is difficult to construct a long-term effective time cycle. It is necessary to ensure that the fire area has image availability in line with the cycle range, and the selection of cycle is also difficult. Based on the spatial comparison built by the contextual method, this MT-contextual method compares the information of spatial comparison with time sequence. This not only improves the spatial high-temperature pixels (factories, etc.) that cannot be eliminated by spatial comparison, but also solves the problem of constructing long-term time series.

In MT-contextual method, the comparison in time series is no longer the brightness temperature of burning pixels. Fig. 5 shows the pixel brightness temperature in the dynamic window during and before the fire. In order to see the change of pixel timing, a small fire on October 24, 2017 is selected. The Yellow pixel (value 0) is the invalid background pixel and the red area is the fire pixel. The fire area is not affected by cloud image, and there are many effective adjacent pixels available. In order to observe the pixel changes before and after combustion, the pixels corresponding to August 24 and October 24 are marked, as shown in Fig. 5(b). According to the pixel brightness temperature value in the figure, it can be seen that the temperature increases in summer in August, and the surface temperature increases significantly as a whole. If only comparing the fire pixels, the brightness temperature value during combustion does not increase significantly compared with that before combustion, and the algorithm is unstable. The establishment of time series period needs to consider this kind of problem, and the suitable period is difficult. When the MT-contextual method compares the spatial difference (fire pixels minus adjacent effective pixels), it can be found that the whole surface temperature in August will increase with the exposure of the sun in summer. At this time, the brightness temperature difference between fire pixels and adjacent pixels in August is very small, but when a fire occurs in October, the difference is very large, even in two seasons with different temperatures, and the spatial difference also has significant changes in time series. The improved algorithm can completely ignore the increase and decrease of surface temperature caused by seasonal changes. Any time before combustion can be selected to construct time series. Ideally, cloud free high-quality images with similar time before combustion are most preferred to avoid the error impact caused by the change of surface type on the establishment of time series.

*3) Description of Algorithm Details:* It can be seen from the above discussion that the fire pixel is obviously different from the other pixels in terms of the temperature difference considered. The following equation provides a quantitative description of the situation:

$$T_i > 360\text{K} \tag{6}$$

$$T_i > 320\text{K} \tag{7}$$

$$\begin{cases} \Delta\ \mathrm{T}^{f-h} = \Delta T_f - \Delta T_h \\ \Delta \mathrm{T}^{f-h} > 3\ \cdot (\delta^f T_{bg} - \delta^h T_{bg}) \end{cases} \tag{8}$$

where $\Delta T_f$ and $\Delta T_h$ is the central fire pixel minus adjacent effective pixel difference in dynamic window [calculated value of spatial effective comparison pixels, formula (5)] at the time of fire and when there is no fire; $\delta^f T_{bg}.\delta^h T_{bg}$, respectively, represents the standard deviation of the brightness temperature of the background pixel in the dynamic window between the current ignition time and no ignition time. Condition (6) and (7) is similar to the "absolute threshold test," and the absolute

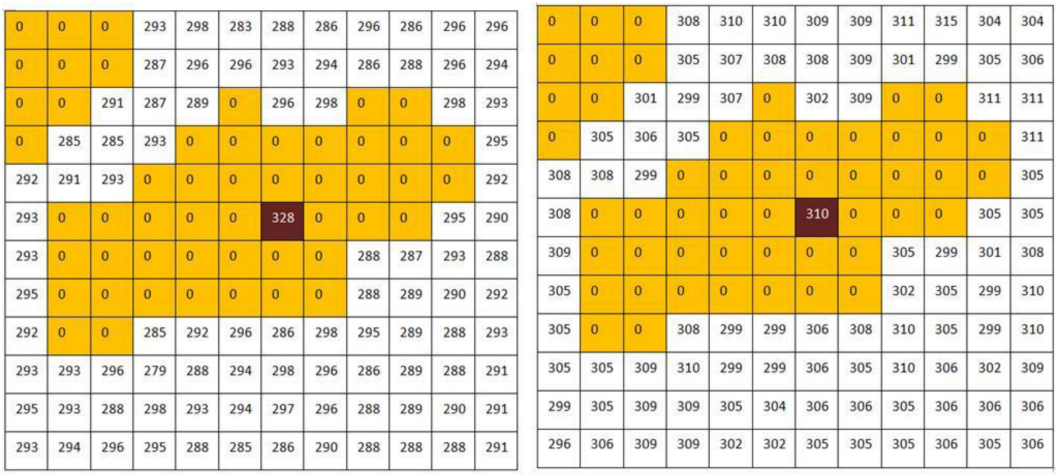

| | | | | | | | | | | | |
|---|---|---|---|---|---|---|---|---|---|---|---|
| 0 | 0 | 0 | 293 | 298 | 283 | 288 | 286 | 296 | 286 | 296 | 296 |
| 0 | 0 | 0 | 287 | 296 | 296 | 293 | 294 | 286 | 288 | 296 | 294 |
| 0 | 0 | 291 | 287 | 289 | 0 | 296 | 298 | 0 | 0 | 298 | 293 |
| 0 | 285 | 285 | 293 | 0 | 0 | 0 | 0 | 0 | 0 | 0 | 295 |
| 292 | 291 | 293 | 0 | 0 | 0 | 0 | 0 | 0 | 0 | 0 | 292 |
| 293 | 0 | 0 | 0 | 0 | 0 | 328 | 0 | 0 | 0 | 295 | 290 |
| 293 | 0 | 0 | 0 | 0 | 0 | 0 | 0 | 288 | 287 | 293 | 288 |
| 295 | 0 | 0 | 0 | 0 | 0 | 0 | 0 | 288 | 289 | 290 | 292 |
| 292 | 0 | 0 | 285 | 292 | 296 | 286 | 298 | 295 | 289 | 288 | 293 |
| 293 | 293 | 296 | 279 | 288 | 294 | 298 | 296 | 286 | 289 | 288 | 291 |
| 295 | 293 | 288 | 298 | 293 | 294 | 297 | 296 | 288 | 289 | 290 | 291 |
| 293 | 294 | 296 | 295 | 288 | 285 | 286 | 290 | 288 | 288 | 288 | 291 |

(a)

| | | | | | | | | | | | |
|---|---|---|---|---|---|---|---|---|---|---|---|
| 0 | 0 | 0 | 308 | 310 | 310 | 309 | 309 | 311 | 315 | 304 | 304 |
| 0 | 0 | 0 | 305 | 307 | 308 | 308 | 309 | 301 | 299 | 305 | 306 |
| 0 | 0 | 301 | 299 | 307 | 0 | 302 | 309 | 0 | 0 | 311 | 311 |
| 0 | 305 | 306 | 305 | 0 | 0 | 0 | 0 | 0 | 0 | 0 | 311 |
| 308 | 308 | 299 | 0 | 0 | 0 | 0 | 0 | 0 | 0 | 0 | 305 |
| 308 | 0 | 0 | 0 | 0 | 0 | 310 | 0 | 0 | 0 | 305 | 305 |
| 309 | 0 | 0 | 0 | 0 | 0 | 0 | 0 | 305 | 299 | 301 | 308 |
| 305 | 0 | 0 | 0 | 0 | 0 | 0 | 0 | 302 | 305 | 299 | 310 |
| 305 | 0 | 0 | 308 | 299 | 299 | 306 | 308 | 310 | 305 | 299 | 310 |
| 305 | 305 | 309 | 310 | 299 | 299 | 306 | 305 | 310 | 306 | 302 | 309 |
| 299 | 305 | 309 | 309 | 305 | 304 | 306 | 306 | 305 | 306 | 306 | 306 |
| 296 | 306 | 309 | 309 | 302 | 302 | 305 | 305 | 305 | 306 | 305 | 306 |

(b)

Fig. 5 Brightness temperature value in dynamic window of fire pixel and non fire pixel. The fire was selected on October 24, 2017 and verified by Landsat series satellite images, and the longitude and latitude information was 45°23'44.11"N,132°9'24.79"E. (a) October 24, 2017. (b) August 24, 2017.

threshold standard is the same as that used in the original algorithm [46]. Equation (6) is the absolute threshold of the daytime situation, while (7) is the judgment condition at night. Expression pixels that can reach the absolute threshold condition can be directly regarded as fire pixels. Equation (8) is the core of the algorithm. Based on the obtained spatial differences, the differences at different times were compared. The selection of factor 3 in test (8) was mainly based on the continuous derivation of the original algorithm [41]. It can be regarded as a fire pixel when it meets the absolute threshold or test (8).

## IV. Results and Discussion

To quantitatively analyze the accuracy and effectiveness of the MT-contextual method, four target regions were selected. The verification work in this article aims to test the accuracy of the timing improvement algorithm and show that it is better than the contextual method applied to the research data (GF-4). In order to achieve these two goals, the MODIS active fire product (MOD14A1-C6) were used for feasibility analysis and the results obtained using the previous GF-4 algorithm were used compared and analyzed, but the detailed evaluation of the algorithm requires a higher spatial resolution scene. Therefore, Landsat data including enhanced thematic mapper plus (ETM +) and operational land imager (OLI) data were used to evaluate the detailed results. Landsat series satellites were used to quantitatively evaluate and verify the fire detection of medium-resolution imaging spectrometer and Geostationary Operational Environment Satellite [35]–[37]. In order to further explore the detection ability of these sensors, relevant algorithms were studied and developed [38], [39]. In this article, Landsat series satellites can be used as indicators for detailed evaluation of algorithm accuracy. With the support of color composites, the burn situation can also be clearly seen in the map through visual interpretation. Differences in imaging time may affect the results, but these data can still provide sufficient fire event information. Active fire events including obvious burn scars can also be used to evaluate cumulative detection result

### A. Comparison With MODIS Products

In recent years, aiming at the research of wildfire identification, MODIS fire thermal anomaly products have been used in scientific research projects and practical operation. In this article, the MOD14A1 product is used as the certification of fire detection results. In this section, the MOD14A1 product is also used as the reference image with 100% accuracy. Most satellite algorithms have used the 10.5–12.4 $\mu$m band to separate the active fire from its nonfire background. Due to the lack of information in the 10.5–12.4 $\mu$m band of the GF-4 satellite, the accuracy of the contextual method used by GF-4 cannot match that of other satellites. Fig. 6(a) and (b), respectively, shows two fire cases in the study area of Heilongjiang on April 9, 2017. Both fires were identified as fire alarms in MOD14A1 products. In order to ensure their reliability, the article was verified by high-resolution images (Landsat ETM +) to ensure that small fires were present. The algorithm in this article (MT-contextual) was used to identify the fire alarm in this area. The MOD14A1 product was compared with the identification results of the algorithm. The spatial resolution of MOD14A1 product is 1 km, and the coverage is large. Due to the influence of satellite shooting angle and resolution, the images cannot be completely superimposed, but it can still be used as the control image for feasibility analysis. Through superposition and comparison, the MT-contextual method accurately identified this small and cold active fire. The construction of timing makes the recognition effect unaffected by the lack of channel information. GF-4 of mid-infrared channel with 400 m spatial resolution realizes accurate spatial positioning. The superposition of burn area to a certain extent shows the feasibility of the MT-contextual method.

### B. Comparison With Contextual Method

In the comparison with the previous section, the MT-contextual method in this article was verified, and was consistent with the recognition effect of other multichannel information satellites. In this section, we mainly discuss the recognition accuracy of the MT-contextual method and contextual method

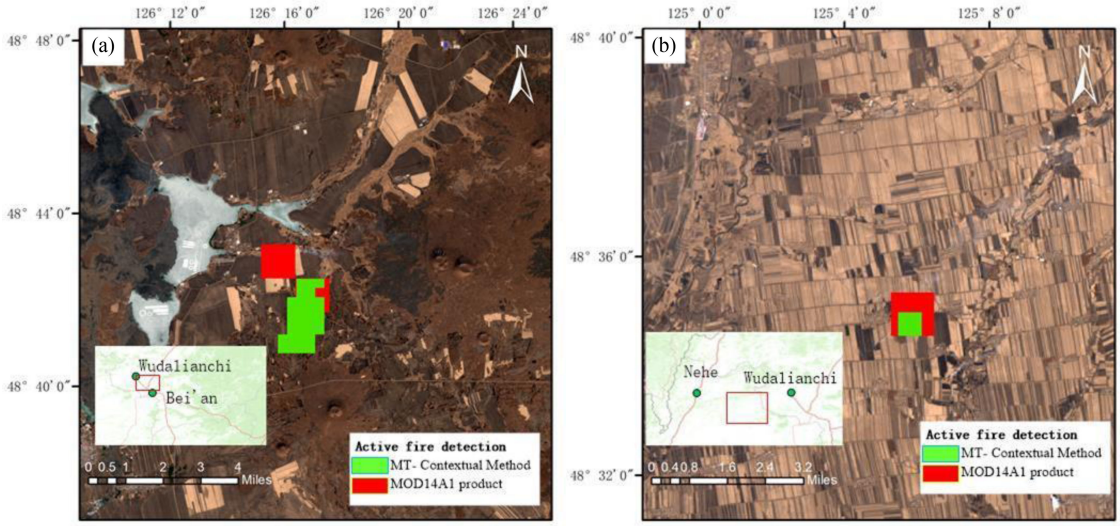


Fig. 6. Compared with MODIS products, the background is created by Landsat.ETM+ images composed of temporal context method and mod14a1 products. The results are marked with different colors. As shown in the location map, fire A occurred on April 9, 2017, with latitude and longitude of 48°41'21.82"N, 126°16'14.91"E, fire B occurred on April 9, 2017; its latitude and longitude are 48°34'30.69"N, 125°5'27.49"E.

TABLE II
STATISTICS OF ALGORITHM DETECTION RESULTS

| Target area | Imaging time | Accuracy[a] | | Commission errors[b] | | Omission error[c] | |
|---|---|---|---|---|---|---|---|
| | | MT- Contextual | Contextual | MT- Contextual | Contextual | MT- Contextual | Contextual |
| Section 1 Australia | 2019/11/18 | 100% | 88.66% | 67.46% | 64.88% | 8.36% | 11.23% |
| | 2019/11/19 | 97.61% | 64.88% | 2.6% | 43.24% | 0 | 0 |
| | 2019/11/20 | 96.88% | 86.21% | 28.36% | 79.23% | 0 | 2.88% |
| Section 2 Heilongjiang | 2017/04/09 | 92.33% | 51.42% | 40% | 64.28% | 19.24% | 19.22% |
| Section 3 Heilongjiang | 2017/10/24 | 98.38% | 88.32% | 89.9% | 91.23% | 24.58% | 38.45% |
| Section 4 Heilongjiang | 2017/10/30 | 91.24% | 29.24% | 52.17% | 64.25% | 17.12% | 33.24% |

[a]Ratio of the number of real fires detected to the number of actual fires
[b]Ratio of the number of false fire pixels detected to the total number of pixels detected
[c]Ratio of the number of missed fires to the number of actual fires
The central pixel positions of the four regions are e150.5_S33.6; E122.6_N45.6; E117.2_N36.2

applied to the research data (GF-4). The overall comparison results are given in Table II, which lists the time range of the scenario. For the accuracy and commission error rate, the true and false detection GF-4 active fire pixels were calculated, respectively. Any Landsat burn marks without corresponding GF-4 detection are marked as missing errors.

The first and second columns in the table provide information on the study area and imaging time of their respective GF-4 scenes. As given in Table II, in most cases, the accuracy of the algorithm exceeds 80%. The result of the new algorithm is an improvement on the existing algorithm. In addition to accuracy, errors should also be considered. The error source is mainly due to the loose constraint of threshold setting and the limitation of the number of GF-4 satellite channels used for algorithm detection. In general, although the error rate is still unsatisfactory, compared with the previous algorithms, the multitemporal method produces improved detection results overall, both in improving accuracy and reducing errors.

This section shows several typical fires in Heilongjiang Province and eastern Russia on October 24, 2017. Fig. 7 shows the comparison results of the MT-contextual method and contextual method in typical cases, in which the overlay base map is the 400 m spatial resolution image of GF-4 PMS. In Fig. 7, the plume position is the fire combustion position with obvious combustion traces. The green patch is the fire pixel identified by the improved algorithm, and the red patch is the fire pixel identified by the contextual method. The fire point extraction result of the time series improved algorithm is consistent with the position of smoke plume in the base map, and is not offset by the influence of high-temperature smoke. In the contextual method recognition, the fire point blocked by thick smoke reduces the energy radiated to the satellite sensor. These fires would have been automatically omitted by the previous algorithm whereas the GF-4 multitemporal method succeeded in detecting the sudden fire events. In the left area of Fig. 7(a), the contextual method does not recognize the fire location, and the location offset occurs in the area affected by smoke at Fig. 7(b). The improved MT-contextual method in this article solves the interference of high-temperature heterogeneous pixels in a single scene and the partial influence of high-temperature

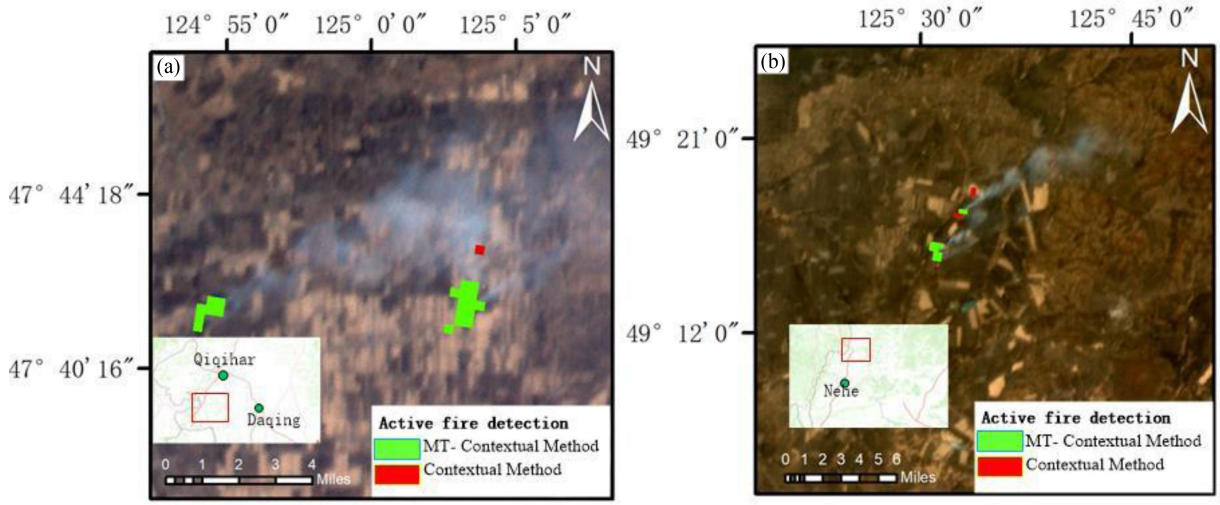


Fig. 7. Compared with contextual algorithm, the results of active fire detection in Heilongjiang on April 7, 2017 are marked with different colors by the temporal context method and the results of context. As shown in the location map, the latitude and longitude of fire in (a) are 47°43'12.31"N, 124° 58'49.70"E, while for fire in (b), the latitude and longitude are 49°18'19.58"N, 125°34'15.68"E.

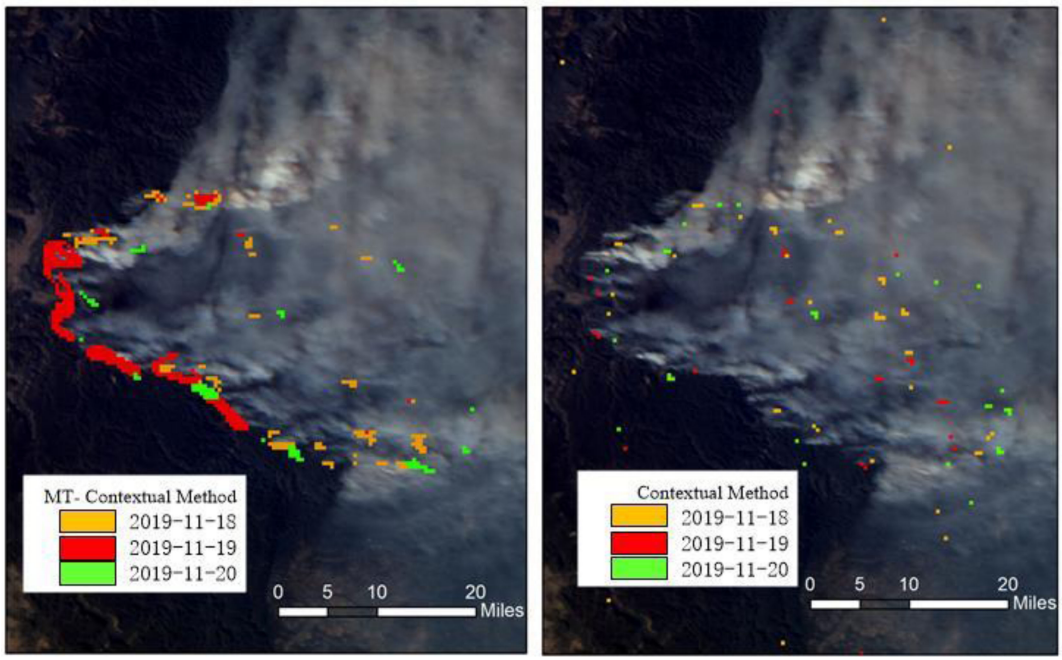


Fig. 8. Fire detection results generated by different algorithms are superimposed on the burn scar.

smoke on the fire location, and successfully detects the active fire location.

### C. Fire Event Cycle Analysis

In this article, the difference in acquisition times between images acquired on the same day prevented the use of traditional methods of assessing the results because the short-term variations in the fire conditions might have seriously affected the quantitative analysis. Besides, the multitemporal method analyzes more data and can be utilized for monitoring the complete cycle of events during a fire.

Fig. 8 shows the comparison results of the contextual method and the MT-contextual method, and reveals the burn scar drawn on the Landsat 8 OLI image. The fire is an Australian mountain fire burning for three consecutive days from November 18–20, 2019. Through visual interpretation of the fire combustion, the fire smoke is large and presents a linear combustion area, Fig 8(a) shows the identification results of the improved MT-contextual method in this article. Fig. 8(b) shows the GF-4 contextual method, which represents the combustion area for three days with three color blocks respectively. Comparative analysis shows that the MT-contextual method color block coincides with the combustion zone more than the contextual method color

block .The filling position of the color blocks in the figure reveals that the improved algorithm is accurate. The consistency of fire description of biomass combustion for many days was improved. The GF-4 contextual method omits some fire pixels in the fire area due to the impacts from smoke and other factors during the fire, and thus, the detection results lose important pixels.

## V. Conclusion

In this article, an active fire detection algorithm, based on GF-4 geostationary satellite multitemporal data, is introduced. PMS and IRS sensors on GF-4 provide data in the spectral range of visible light to mid-infrared. The basic "context" structure of a fire detection algorithm similar to a medium-resolution imaging spectrometer already exists. To improve the existing algorithm, the new algorithm uses multitemporal data and introduces a time-series analysis. This algorithm can be used to eliminate high-temperature heterogeneous points without fire, which cannot be achieved by the contextual method. In recent years, to construct the time series analysis, we need to consider the quantity and quality of the data involved. Usually, both the front and back data are required for calculation, which greatly increases the complexity of calculation and dependence on data. In addition, the quality of continuous data acquired from the satellites has become poor, as too many invalid data outliers lead to difficulty in constructing an accurate time series. Through the combination of space and time, this algorithm reduces the dependence on long-term effective data, and provides a convenient and effective time series construction method for fire detection. It has a relatively high accuracy for fire detection compared to the traditional methods, and the false fire recognition rate is significantly reduced.

Change analysis, based on the change detection method, cannot fully mine the relationship between many multitemporal images; further, the coverage conditions and subtle or long-term changes under climate change cannot be readily separated from the background noise. There are also some ground types with sudden temperature changes that are confused with fire. Solving the easily confused ground is also the focus of future work. At the same time, the goal of this article is global testing. The difference of ground types in different regions may lead to the deviation of threshold. Increasing the judgment of different types of ground in different regions is also the direction of future work.

## References


[1] N. Andela *et al.*, "A human-driven decline in global burned area," *Science*, vol. 356, pp. 1356–1362, 2017.

[2] M. O. Andreae, "Biomass burning: Its history, use and distribution, and its impact on environmental quality in global climate," in *Global Biomass Burning: Atmosphere, Climatic, and Biospheric Implications*, J. Levine, Ed., Cambridge, MA, USA: MIT Press, 1991, pp. 3–21.

[3] D. M. J. S. Bowman, "Fire in the earth system," *Science*, vol. 324, pp. 481–484, 2009.

[4] F. Johnston, "Extreme air pollution events from bushfires and dust storms and their association with mortality in Sydney, Australia 1994–2007," *Environ. Res*, vol. 111, pp. 811–816, 2011.

[5] M. Natarajan, "Radiative forcing due to enhancements in tropospheric ozone and carbonaceous aerosols caused by Asian fires during spring 2008," *J. Geophys. Res. Atmos.*, vol. 117, 2012.

[6] G. R. van der Werf, "Continental-scale partitioning of fire emissions during the 1997 to 2001 El Nino/La Nina period," *Science*, vol. 303, pp. 73–76, 2004.

[7] A. Voulgarakis, and R. D. Field, "Fire influences on atmospheric composition, air quality and climate," *Current Pollut. Rep.*, vol. 1, pp. 70–81, 2015.

[8] M. J. Wooster, "Meteosat SEVIRI fire radiative power (FRP) products from the land surface analysis satellite applications facility (LSA SAF) – Part 1: Algorithms, product contents and analysis," *Atmos. Chem. Phys. Discuss.*, vol. 15, pp. 15831–15907, 2015.

[9] J. W. Kaiser, "Biomass burning emissions estimated with a global fire assimilation system based on observed fire radiative power," *Biogeosciences*, vol. 9, pp. 527–554, 2012.

[10] M. O. Andreae, "Emission of trace gases and aerosols from biomass burning – An updated assessment," *Atmos. Chem. Phys.*, vol. 19, pp. 8523–8546, 2019.

[11] M. D. Flannigan, "Forest fire monitoring using NOAA Satel-lite AVHRR," *Can. J. Forest Res.*, vol. 16, no. 5, pp. 975–982, 1986.

[12] M. Nakayama, M. Maki, C. D. Elvidge, and S. C. Liew, "Contextual algorithm adapted for NOAA-AVHRR fire detection in Indonesia," *Int. J. Remote Sens.*, vol. 20, no. 17, pp. 3415–3421, 1999.

[13] C. O. Justice *et al.*, "The MODIS fire products," *Remote Sens. Environ.*, vol. 83, no. 1, pp. 244–262, 2002.

[14] D. Cheng, J. Rogan, L. Schneider and M. Cochrane, "Evaluating MODIS active fire products in subtropical Yucatan forest," *Remote Sens. Lett.*, vol. 4, no. 5, pp. 455–464, 2013.

[15] A. Abuelgasim and R. Fraser, "Day and night-time active fire detection over North America using NOAA-16 AVHRR data," in *Proc. IEEE Int. Geosci. Remote Sens. Symp.*, 2002, vol. 3, pp. 1489–1491.

[16] K. A. Kalpoma and J. I. Kudoh, "A new algorithm for forest fire detection method with statistical analysis using NOAA AVHRR images," *Int. J. Remote Sens.,* vol. 27, no. 18, pp. 3867–3880, 2006.

[17] J. Dozier, "A method for satellite identification of surface temperature fields of subpixel resolution," *Remote Sens. Environ.*, vol. 11, pp. 221–229, 1981.

[18] L. Giglio *et al.*, "Evaluation of global fire detection using simulated A VHRR infrared data," *Int. J. Remote Sens.*, vol. 20, no. 10, pp. 1947–1985, 1999.

[19] E. M. Fuchs, "Fire monitoring the ues of medium resolution satellites (AVHRR, MODIS, TET) for long time series processing and the implementation in user driven application andsercices," *Int. Arch. Photogramm., Remote Sens. Spatial Inf. Sci.*, vol. XL-7/W3, no. 7, pp. 797–804, 2015.

[20] L. Giglio *et al.*, "A multi-year active fire dataset for the tropics derived from TRMM VIRS," *Int. J. Remote Sens.*, vol. 24, no. 22, pp. 4505–4525, 2003.

[21] L. Giglio *et al.*, "The collection 6 MODIS active fire detection algorithm and fire products," *Remote Sens. Environ.*, vol. 178, pp. 31–41, 2016.

[22] P. H. Freeborn *et al.*, "Development of a virtual active fire product for Africa through a synthesis of geostationary and polar orbiting satellite data," *Remote Sens. Environ.*, vol. 113, pp. 1700–1711, 2009.

[23] Y. M. Rao, C. Wang, and H. G. Huang, "Forest fire monitoring based on multisensory remote sensing techniques in Muli County, Sichuan Province," *J. Remote Sens.,* vol. 24, no. 5, pp. 559–570, 2020.

[24] Q. Li *et al.*, "Monitoring of the fire in Muli County on March 28, 2020, based on high temporal-spatial resolution remote sensing techniques," *Nat. Hazards Res.*, vol. 1, no. 1, pp. 20–31, 2021.

[25] W. Schroeder *et al.*, "The new VIIRS 375 m active fire detection data product: Algorithm description and initial assessment," *Remote Sens. Environ.,* vol. 143, pp. 85–96, 2014.

[26] M. Amraoui *et al.*, "Detection and monitoring of African vegetation fires using MSG-SEVIRI imagery," *Remote Sens. Environ.*, vol. 114, no. 5, pp. 1038–1052, 2010.

[27] M. Amraoui, C. C. DaCamara, and J. M. C. Pereira, "Detection and monitoring of African vegetation fires using MSG-SEVIRI imagery," *Remote Sens. Environ.*, vol. 114, pp. 1038–1052, 2010.

[28] Y. Govaerts, Wooster, P. M. Freeborn, A. Lattanzio, and G. Roberts., "MSG SEVIRI fire radiative power (FRP) characterisation. Algorithm theoretical basis document," 2010.

[29] M. Gao and J. Li. "Automatic registration of GF-4 PMS: A high resolution multi-spectral sensor on board A satellite on geostationary orbit," *ISPRS Int. Arch. Photogramm. Remote Sens. Spatial Inf. Sci.,* vol. XLII-3, pp. 359−362, 2018.

[30] I. A. Csiszar, J. T. Morisette, and L. Giglio, "Validation of active fire detection from moderate-resolution satellite sensors: The MODIS example in Northern Eurasia," *IEEE Trans. Geosci. Remote Sens.*, vol. 44, no. 7, pp. 1757–1764, Jul. 2006.

[31] W. Wang *et al.*, "An improved algorithm for small and cool fire detection using MODIS data: A preliminary study in the southeastern United States," *Remote Sens. Environ.*, vol. 108, no. 2, pp. 163–170, 2007.
[32] Y. Xie *et al.*, "Smoke plume detection in the eastern United States using MODIS," *Int. J. Remote Sens.*, vol. 28, no. 10, pp. 2367–2374, 2007.
[33] W. Schroeder *et al.*, "Validation of GOES and MODIS active fire detection products using ASTER and ETM+ data," *Remote Sens. Environ.*, vol. 112, no. 5, pp. 2711–2726, 2008.
[34] S. W. Maier *et al.*, "Sensitivity of the MODIS fire detection algorithm (MOD14) in the savanna region of the Northern Territory, Australia," *ISPRS J. Photogramm.*, vol. 76, pp. 11–16, 2013.
[35] Y. Govaerts *et al.*, "MSG SEVIRI fire radiative power (FRP) characterisation," 2010.
[36] E. M. Prins, *et al.*, "An overview of GOES-8 diurnal fire and smoke results for SCAR-Band 1995 fire season in South America," *J. Geophys. Res.*, vol. 103, pp. 31821–31835, 1998.
[37] W. Xu *et al.*, "New GOES imager algorithms for cloud and active fire detection and fire radiative power assessment across North, South and Central America," *Remote Sens. Environ.*, vol. 114, no. 9, pp. 1876–1895, 2010.
[38] G. J. Roberts and M. J. Wooster, "Fire detection and fire characterization over Africa using Meteosat SEVIRI," *IEEE Trans. Geosci. Remote Sens.,* vol. 46, no. 4, pp. 1200–1218, Apr. 2008, doi: 10.1109/TGRS.2008.915751.
[39] B. Zhukov *et al.*, "Spaceborne detection and characterization of fires during the Bi-spectral infrared detection (BIRD) experimental small satellite mission (2001–2004)," *Remote Sens. Environ.*, vol. 100, no. 1, pp. 29–51.
[40] G. Mazzeo *et al.*, "A multi-temporal robust satellite technique (RST) for forest fire detection analysis of multi-temporal remote sensing images," in *Proc. Int. Workshop Anal. Multitemporal Remote Sens. Images*, 2007, pp. 1–6.
[41] D. P. Roy, Y. Jin, P. E. Lewis, and C. O. Justice, "Prototyping a global algorithm for systematic fire-affected area mapping using MODIS time series data," *Remote Sens. Environ.,* vol. 97, no. 2, pp. 137–162, 2005.
[42] R. Lasaponara, V. Cuomo, M. F. Macchiato, and T. Simoniello, " A self-adaptive algorithm based on AVHRR multitemporal data analysis for small active fire detection," *Int. J. Remote Sens.,* vol. 24, no. 8, pp. 1723–1749, 2003.
[43] K. Kushida, "Detection of active wildland fires using multitemporal MODIS images," *IEEE Trans. Geosci. Remote Sens.,* vol. 7, no. 2, pp. 301–305, Apr. 2010, doi: 10.1109/LGRS.2009.2034029.
[44] D. R. Panuju, B. H. Trisasongko, B. Susetyo, M. A. Raimadoya, and B. G. Lees, "Historical fire detection of tropical forest from NDVI time-series data: Case study on Jambi, Indonesia," *J. Math. Fundam. Sci.,* vol. 42, no. 1, pp. 49–66, 2010.
[45] L. Lin *et al.*, "A Spatio-temporal model for forest fire detection using HJ-IRS satellite data," *Remote Sens*, vol. 8, no. 5, 2016.
[46] Y. J. Kaufman, "Potentialglobal fire monitoring from EOS-MODIS," *J. Geophys. Res.*, vol. 103, pp. 32215–32238, 1998.